

Experimental study of photon-echo size in optically thick media

T. Wang, C. Greiner, J. R. Bochinski, and T. W. Mossberg

Department of Physics and Oregon Center for Optics, University of Oregon, Eugene, Oregon 97403

(Received 22 February 1999)

We have studied the effect of generative-pulse amplitude, spatial profile, and temporal character as well as medium optical thickness on the power of photon and stimulated echoes. Working in atomic Yb vapor, photon echoes are observed that, absent material relaxation, are more powerful than the first generative pulse, thereby exceeding typically expected photon-echo powers by approximately two orders of magnitude. Factors crucial to the generation of powerful echoes identified through Maxwell-Bloch simulation are experimentally confirmed. [S1050-2947(99)51308-5]

PACS number(s): 42.50.Md, 42.65.-k

Since their first observation in 1964 [1] optical coherent transients have held intrinsic interest from a phenomenological point of view, have proven useful as a tool for measuring various material parameters, and have received attention as the basis of various proposed signal processing [2–5], information storage [6–8], and optical beam control devices [9]. In many envisioned applications, the output signal is either a reproduction or a processed modification of one generative input signal. We call the input signal, which is in some manner reproduced, the data signal. The power difference between the data and output signals is important in the device context as it represents an insertion loss. The widespread belief that optical coherent transient signals regenerate only a small portion of the energy contained in a data signal has contributed to the perception that transient processes have limited practical applicability.

We undertake here an experimental and theoretical study of photon and stimulated echo power compared to that of input data signals. The specific concern is to identify those conditions that lead to the production of echo signals having a power comparable to or larger than the data signal. Interestingly, it is found that echoes can be generated that have powers as high or higher than associated data signals, provided a number of parameters are controlled. We note that various approaches were previously suggested to enhance the echo signal size, including using inverted media [10], placing the sample in an optical cavity [11], and utilizing auxiliary optical amplification [12].

An important parameter controlling maximal echo size is the optical thickness of the generative medium [13–16]. Limited by a variety of assumptions, it has been believed that echo sizes are maximized at $\alpha L \approx 1$ [15], where α is the medium's absorption coefficient at the generative signal's frequency and L is the medium's length. Only recently has work based on the integration of the Maxwell-Bloch equations shown deviation from this long standing notion [17–19], indicating that $\alpha L > 1$ uniquely provides for echo/data signal power ratios (echo efficiencies) having values up to, and exceeding, unity. Interestingly, previous experimental echo studies in optically thick media, including gas [20] and ion-doped optical fiber [21,22], have demonstrated echo efficiencies of only 10% or less even after accounting for material relaxation. We note that the $\alpha L > 1$ domain has been shown to support certain characteristic behaviors, including

αL -dependent nonexponential decay [23,24] and multiple echoes [22,25], as well as echo timing and shape modifications [25].

Both photon echoes and stimulated echoes are studied in our experiment. There are two (three) generative input pulses in the photon-echo (stimulated echo) case, and the first (second) generative pulse is here called the data pulse. The other input pulses are called reference pulses and usually contain more energy than the data pulse. The echo power efficiency E_e is the ratio of the peak echo power P_e to the peak data pulse power P_d measured before the generative medium. We use θ_i and τ_i to represent the pulse area (at the center of the transverse spatial profile) and temporal width of the i th generative pulse, and τ_{ij} to represent the time delay between the centers of the i th and j th generative pulses.

In our experiment the output of a ring dye laser is tuned to the 556-nm (1S_0 - 3P_1) transition of ^{174}Yb with a radiative lifetime of 875 ns. This atomic system was first employed in the photon-echo study of atomic-coherence preserving collisions [26]. The dye laser output is gated by a 12-ns-switching-time, acousto-optic modulator to produce echo-generative pulses. The generative pulses are spatially filtered, collimated to a full width at half maximum (FWHM) diameter $D_0 \approx 4.5$ mm, and passed through an iris of diameter D_I (see Fig. 1) whose aperture plane is imaged with unity spatial and angular magnification into the center of a stainless-steel gas cell that contains Yb in its natural isotopic abundance. With the iris aperture set to $D_I \approx 2$ mm, the value used except where otherwise noted, pulses with a transverse intensity variation of less than 15% are realized. A quarter-wave plate circularly polarizes the pulses prior to their entry into the Yb cell. A magnetic field of ≈ 10 G applied along the optical propagation direction provides definition to the quantization scheme wherein the circularly polarized generative pulses couple the ground state to only one of the three m_J

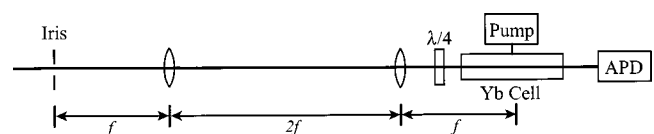


FIG. 1. Schematic of beam-shaping input optics, vapor cell, and detection. APD, avalanche photodiode; $\lambda/4$, quarter-wave plate; pump, diffusion pump.

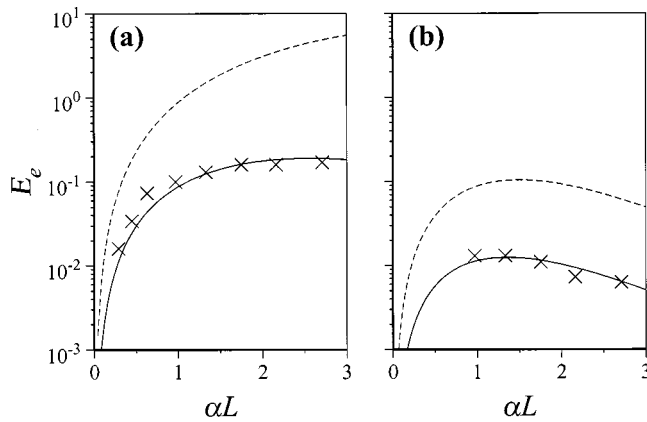


FIG. 2. Photon-echo power efficiency E_e versus αL for (a) $\theta_2 = \pi$, and (b) $\theta_2 = \pi/2$. The solid (dashed) line represents simulation results that include (exclude) material relaxation. The \times 's represent experimental results.

levels in the 3P_1 state. The output signal is detected by an avalanche photodiode and electronically amplified. The Yb cell temperature controls the Yb vapor pressure within the cell and hence the medium's optical thickness αL . Maximum achievable beam-center resonant Rabi frequencies were in the range of 7–10 MHz.

In Fig. 2, we compare measured and simulated photon-echo efficiencies as a function of αL for $\theta_2 = \pi$ and $\pi/2$. The simulation results are obtained by numerical integration of the Maxwell-Bloch equations [19]. The solid (dashed) lines represent simulations that account for (exclude) relaxation in the medium. The \times 's represent measured values. The relaxation model includes the spontaneous radiative decay of the upper atomic state and the loss of atomic population in the active volume arising from transverse atomic motion. The latter relaxation effect has been investigated in Refs. [27] and [28] and is here statistically modeled based on a Maxwell-Boltzmann velocity distribution. Collisional effects are ignored. For $\alpha L > 1$, the relaxation model considered predicts nonexponential decay of the echo signal as a function of τ_{12} . This effect has been noted previously [23] and must be considered in deducing unrelaxed echo power. The experimental parameters are $\tau_1 = 150$ ns, $\tau_2 = 50$ ns and $\tau_{12} = 600$ ns. The energy content of the input data pulse is approximately 0.8% that of the input reference pulse.

The experimental and relaxation-inclusive simulations (solid lines) are in agreement. With this verification of the theoretical model it is reasonable to conclude that efficiencies given by the dashed line would be observed in the absence of the radiative and transit time relaxation mechanisms. Note that for $\alpha L > 1$ and $\theta_2 = \pi$ echo efficiencies exceed unity.

We now investigate the population inversion before and after emission of the photon echo. In Fig. 3 the population inversion w is plotted as a function of atom-field detuning Δ for times after the second generative pulse but prior to the echo (upper dashed line) and after the echo (upper solid line). Also shown is the difference δw between the upper dashed and solid lines (lower solid line). The horizontal scale is normalized to Δ_1 , the FWHM of the data pulse's power spectrum. The oscillatory character in the post-echo population inversion arises from the fact that the echo field-medium

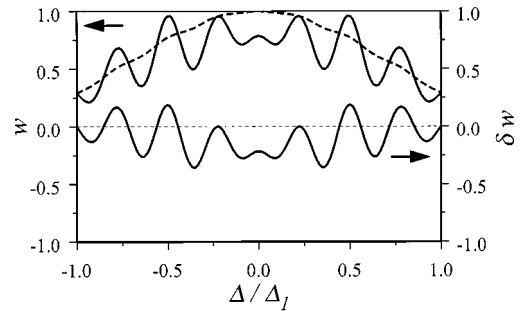


FIG. 3. Atomic population inversion w versus detuning Δ . Upper dashed line, w before photon echo (after second pulse). Upper solid line, w after the photon echo generation. Lower solid line, change of population inversion δw after the photon echo generation. The horizontal scale is normalized to Δ_1 , the FWHM of the data pulse's power spectrum.

interaction is coherent. The parameters used in the simulation here are $\alpha L = 3$, $\theta_1 = \pi/20$, $\theta_2 = \pi$, and $\tau_1/\tau_2 = 10$. No relaxation is considered in this simulation.

Figure 3 shows that the generative pulses create a positive population inversion and that the inversion is depleted in the course of echo emission. Energy is thus transferred from the generative pulses (primarily the second) to the echo via the medium. Further simulations show that the generative-pulse-to-echo energy transfer occurs only when $w > 0$ over most of the data pulse bandwidth. Substantial increase of echo size is possible in an optically thick medium, as shown in Fig. 2(a). However, if the generative pulses are not strong enough to invert most atoms in the data pulse bandwidth, then the medium remains absorptive and attenuates the echo. This effect is evident in Fig. 2(b), where the generative pulses have insufficient area to produce substantial inversion. Further simulation also indicates that the energy transfer process is insensitive to the relative phase between the generative pulses. With otherwise identical parameters, changing the relative phase over a range of 0 to π yields no perceivable difference in echo power efficiency. It should be pointed out that the energy transfer process is not a simple laser gain effect. Laser gain describes an incoherent atom-field interaction. In the present case, the full atomic coherence is preserved. It is only the average over the atom-field detuning that removes dependence on the generative pulse relative phase.

As pointed out in our previous simulation study [19], the relative temporal widths of the first and second generative pulses have a strong effect on echo power efficiency. In Fig. 4 we explore the effect of the width ratio τ_1/τ_2 on the photon-echo power efficiency. The observed relative echo efficiency is plotted versus τ_1/τ_2 with fixed $\tau_2 = 50$ ns for two different αL values. Here $\theta_2 \approx \pi$. The first generative pulse power is fixed and $\theta_1 \approx (\tau_1/400)$ ns. The echo power efficiency increases with τ_1/τ_2 at a rate that increases with αL . This is consistent with our previous prediction [19] that the condition $\tau_2 \ll \tau_1$ is essential to efficient echo generation. Large τ_1/τ_2 implies that the bandwidth of the second generative pulse exceeds the one of the first generative (data) pulse and therefore rephases its entire spectral content.

The variation of echo efficiency as a function of

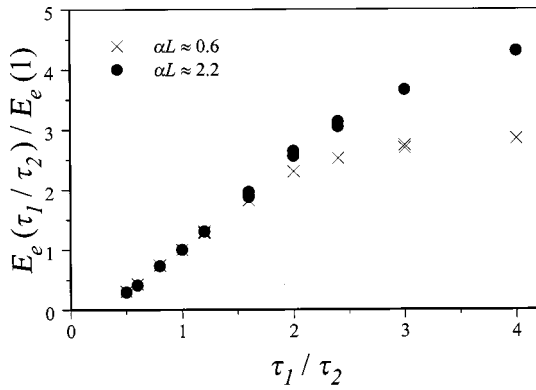


FIG. 4. Relative photon-echo power efficiency versus the width ratio of the two generative pulses, τ_1/τ_2 . The value of τ_2 is fixed at 50 ns and $\theta_2 \approx \pi$.

generative-pulse transverse-intensity profile is shown in Fig. 5. In Fig. 5(a) we plot the observed relative echo power efficiency versus D_1/D_0 at two different αL values. When $D_1/D_0 \leq 1$ ($D_1/D_0 > 1$), the generative pulses have a top-hat-like (Gaussian-like) transverse intensity profile. Measurements were obtained with beam-center areas $\theta_1 \approx 0.3$ and $\theta_2 \approx \pi$, generative pulse durations $\tau_1 = 90$ ns and $\tau_2 = 50$ ns, and a delay of $\tau_{12} = 600$ ns. According to our previous simulations [19], generative fields with a top-hat-like transverse intensity profile generally yield high echo power efficiency. To remove transit-time relaxation effects that vary with D_1/D_0 and complicate the data of Fig. 5(a), we show in Fig. 5(b) the relative relaxation-compensated echo power efficiency E_e^* , calculated using the data in Fig. 5(a) and echo decay rates estimated from experimentally measured echo size versus τ_{12} . This correction does not account for nonexponential behavior in the variation of echo power versus τ_{12} and is thus approximate. For both αL values, the echo efficiency is found to be approximately 2–3 times higher with the smallest D_1/D_0 (top-hat-like) than with the largest D_1/D_0 (Gaussian-like). As discussed elsewhere [19], the dependence of echo efficiency on transverse intensity profile

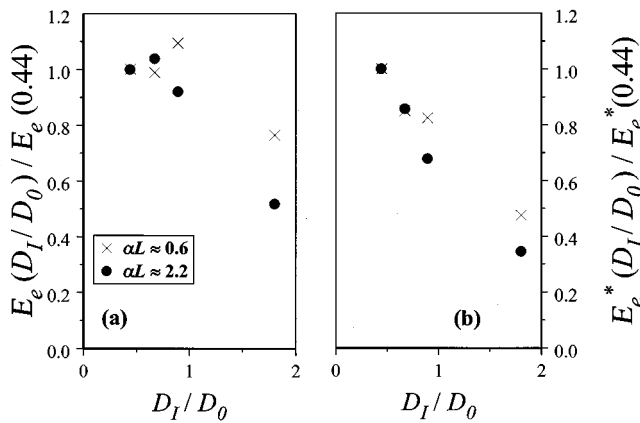


FIG. 5. (a) Relative photon-echo power efficiency versus beam transverse profile for two αL values. $D_1/D_0 \approx 0.44$ corresponds to $D_1 \approx 2$ mm. (b) Same as (a), except that relaxation-compensated values are used.

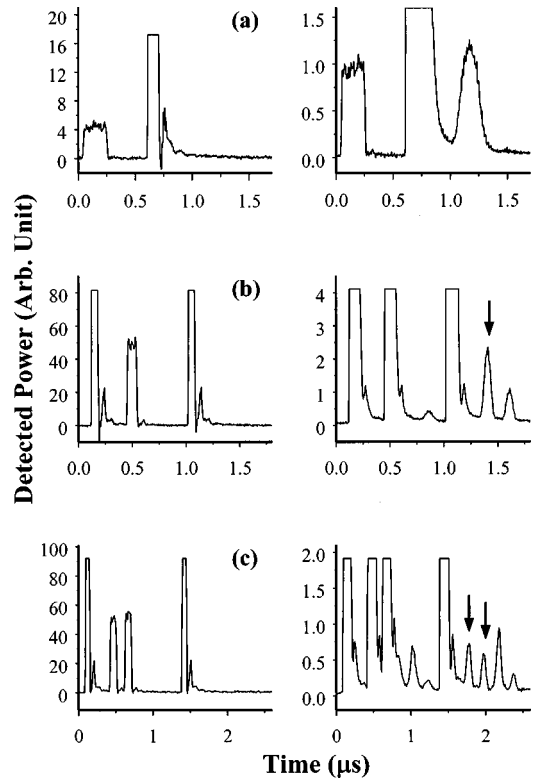


FIG. 6. Single-event recordings of excitation pulses and (a) photon echo, (b) stimulated echo, and (c) stimulated echo where the data (second) field is comprised of subpulses. The right (left) traces are recorded with the laser frequency overlapped with (outside of) the atomic absorption profile. In (b) and (c) the stimulated echoes are marked by arrows. All reference fields as well as the data fields of the right traces in (b) and (c) are off the vertical scale. The auxiliary structure immediately following each input pulse is caused by the modulation electronics.

follows from the need for the second generative pulse to have a specific area to ensure maximal echo efficiency. This is not possible with a spatially varying transverse intensity profile.

In Figs. 6(a) [6(b)], we show the single-event recordings of the transmitted optical power versus time of two (three) generative input fields and the respondent photon (stimulated) echoes. In each plot the right (left) trace is recorded when the laser frequency is resonant with (well detuned from) the Doppler broadened atomic resonance. The left traces thus correspond to the unattenuated generative fields. For Fig. 6(a), where $\tau_1 = 210$ ns, $\tau_2 = 60$ ns, $\tau_{12} = 500$ ns, $\theta_1 \approx 0.4$, $\theta_2 \approx \pi$, and $\alpha L \approx 1.6$, one finds in relative units a peak echo power P_e of ~ 1.1 and a peak data pulse power P_d of ~ 5 . When the echo power is multiplied by a factor to compensate for relaxation effects, the corresponding echo efficiency is 1.7. For Fig. 6(b) where the parameters are $\tau_1 = 35$ ns, $\tau_2 = 90$ ns, $\tau_3 = 38$ ns, $\tau_{12} = 350$ ns, $\tau_{23} = 550$ ns, $\theta_1 \approx 1.8$, $\theta_2 \approx 0.45$, $\theta_3 \approx 2.0$, and $\alpha L \approx 1.6$, one finds that in relative units $P_e \approx 2.0$ and $P_d \approx 50$. Compensation for medium relaxation gives a stimulated echo efficiency of 0.7.

In Fig. 6(c), with left and right traces as in Figs. 6(a) and 6(b), we show the stimulated echo generated by a data (second) field comprised of a multitude of subpulses. The subpulses, representative of binary data, are clearly reproduced

in the echo signal, as indicated by the two arrows. Here $\tau_2 = 90$ ns ($\theta_2 \approx 0.4$) represents the width (area) of each subpulse and $\tau_{12} = 350$ ns ($\tau_{23} = 950$ ns) is the separation between the first subpulse and the first (third) generative field. The separation between the two subpulses is 200 ns. The other parameters are the same as those used in Fig. 6(b). Based on the first subpulse, in relative units, $P_e \approx 0.6$ and $P_d \approx 50$, which after adjusting for relaxation yields a stimulated echo efficiency of 0.7.

In summary, it has been experimentally demonstrated that relaxation-compensated echo powers can be comparable to or larger than input data signal powers, provided the generative medium is optically thick. In the stimulated echo case, efficient echo signals are shown to retain the ability to repro-

duce the temporal profile of a data signal. The generative pulse parameters consistent with efficient echo generation, theoretically predicted elsewhere [19], are now experimentally verified. The medium dynamics that provide for an echo signal to be more energetic than an input data pulse are discussed especially in relation to coherently depleted inversion effects. High efficiency is especially important in potential application areas such as optical time-delayed amplification where data pulse and echo comprise inputs and outputs, while the reference pulse(s) serve the function of a local power source.

We appreciate support from Dr. Alan Craig and the U.S. Air Force Office of Scientific Research under Contract No. F49620-96-1-0259.

-
- [1] N. A. Kurmit, I. D. Abella, and S. R. Hartmann, *Phys. Rev. Lett.* **13**, 567 (1964).
- [2] E. Manykin and S. Zakharov, *Proc. SPIE* **2969**, 64 (1996); V. A. Katulin, A. A. Biryukov, and V. V. Samartsev, *Bull. Acad. Sci. USSR, Phys. Ser.* **53**, 1 (1989).
- [3] Y. S. Bai, W. R. Babbitt, N. W. Carlson, and T. W. Mossberg, *Appl. Phys. Lett.* **45**, 714 (1984).
- [4] E. A. Manykin and N. A. Chernishev, *Proc. SPIE* **1505**, 141 (1991).
- [5] S. Kröll and U. Elman, *Opt. Lett.* **18**, 1834 (1993).
- [6] T. W. Mossberg, *Opt. Lett.* **7**, 77 (1982).
- [7] M. Mitsunaga, *Opt. Quantum Electron.* **24**, 1137 (1992), and references therein.
- [8] X. A. Shen, E. Chiang, and R. Kachru, *Opt. Lett.* **19**, 1246 (1994).
- [9] W. R. Babbitt and T. W. Mossberg, *Opt. Lett.* **20**, 910 (1995); T. Wang, H. Lin, and T. W. Mossberg, *ibid.* **20**, 2541 (1995); X. A. Shen and R. Kachru, *ibid.* **20**, 2508 (1995); T. L. Harris, Y. Sun, R. L. Cone, R. M. Macfarlane, and R. W. Equall, *ibid.* **23**, 636 (1998).
- [10] M. Azadeh and W. R. Babbitt, *Mol. Cryst. Liq. Cryst. Sci. Technol., Sect. A* **291**, 269 (1996).
- [11] T. Wang, C. Greiner, and T. W. Mossberg, *Opt. Lett.* **23**, 1736 (1998).
- [12] B. S. Ham and M. K. Kim, *Appl. Opt.* **33**, 4472 (1994); B. Luo, U. Elman, and S. Kröll, *Opt. Lett.* **23**, 442 (1998).
- [13] A. Compaan and I. D. Abella, *Phys. Rev. Lett.* **27**, 23 (1971).
- [14] G. L. Lamb, Jr., *Rev. Mod. Phys.* **43**, 99 (1971).
- [15] R. Friedberg and S. R. Hartmann, *Phys. Lett.* **37A**, 285 (1971).
- [16] E. L. Hahn, N. S. Shiren, and S. L. McCall, *Phys. Lett.* **37A**, 265 (1971).
- [17] J. T. Manassah and B. Gross, *Opt. Commun.* **140**, 70 (1997).
- [18] M. Azadeh, C. Sjaarda, W. R. Babbitt, and L. Tsang, *Phys. Rev. A* **57**, 4662 (1998).
- [19] T. Wang, C. Greiner, and T. W. Mossberg, *Opt. Commun.* **153**, 309 (1998).
- [20] C. K. N. Patel and R. E. Slusher, *Phys. Rev. Lett.* **20**, 1087 (1968).
- [21] J. Hegarty, M. M. Broer, B. Golding, J. R. Simpson, and J. B. MacChesney, *Phys. Rev. Lett.* **51**, 2033 (1983).
- [22] M. M. Broer and B. Golding, *J. Opt. Soc. Am. B* **3**, 523 (1986).
- [23] R. W. Olson, H. W. H. Lee, F. G. Patterson, and M. D. Fayer, *J. Chem. Phys.* **76**, 31 (1982).
- [24] F. C. Spano and W. S. Warren, *J. Chem. Phys.* **93**, 1546 (1990).
- [25] J. T. Manassah and B. Gross, *Laser Phys.* **4**, 83 (1994); B. Gross and J. T. Manassah, *ibid.* **3**, 612 (1993).
- [26] R. A. Forber, L. Spinelli, J. E. Thomas, and M. S. Feld, *Phys. Rev. Lett.* **50**, 331 (1983).
- [27] J. E. Thomas and R. A. Forber, *Opt. Lett.* **9**, 56 (1984).
- [28] J. L. Cohen and P. R. Berman, *Phys. Rev. A* **54**, 5262 (1996), and references therein.